Nanoscale Electrochemical Patterning Reveals the Active Sites for Catechol Oxidation at Graphite Surfaces

Anisha N. Patel[†], Kim M[c]Kelvey[†‡] and Patrick R. Unwin[†]*

[†]Department of Chemistry and [‡]MOAC Doctoral Training Centre, University of Warwick, Coventry CV4 7AL, United Kingdom.

Supporting Information Placeholder

ABSTRACT: Graphite-based electrodes (graphite, graphene and nanotubes) are used widely in electrochemistry, and there is a long-standing view that graphite step edges are needed to catalyze many reactions, with the basal surface considered to be inert. Herein, this model is tested directly, for the first time, using scanning electrochemical cell microscopy (SECCM) reactive patterning, and shown to be incorrect. Using the electro-oxidation of the catechol, dopamine, as a model process, the reaction rate is measured at high spatial resolution across a surface of highly oriented pyrolytic graphite (HOPG). Oxidation products left behind in a pattern defined by the scanned electrochemical cell, serve as a surface site marker, allowing the electrochemical activity to be correlated directly with the graphite structure at the nanoscale. This process produces tens of thousands of electrochemical measurements at different locations across the basal surface, unambiguously revealing it to be highly electrochemically active, with step edges providing no enhanced activity. This new model of graphite electrodes has significant implications for the design of carbon-based biosensors, and the results are additionally important for understanding electrochemical processes at related sp^2 materials such as pristine graphene and nanotubes.

Carbon electrodes, from graphite to conducting diamond, constitute interesting platforms for electroanalysis and electrocatalysis due to low background currents, wide potential windows, chemical inertness, sensitivity, biocompatibility, low cost and ready availability.[1] They have found particularly wide application for bioelectrochemical analysis, either directly or as supports for electrocatalysts.[2] The introduction of graphene and carbon nanotubes (CNTs) has expanded the range of carbon-based electrode materials, and has enhanced the need for a greatly improved understanding of the electrochemical properties of graphitic materials.

Carbon electrodes are used extensively for the electrochemical detection and analysis of catechols,[1,3] and related molecules, with apparently slow kinetics being found for dopamine (DA) electro-oxidation at basal plane graphite, with peak-to-peak separations as large as 1.2 V (at 0.2 V s^{-1}) in cyclic voltammetry.[4] This has led to such processes being considered to be catalyzed solely by step edges, with the basal surface regarded as being inert.[4,5] Consequently, carbon electrodes used in neuroscience and on biosensing platforms are often designed to maximize step edges.[1c,6] The studies herein show that this model is incorrect for the most studied neurotransmitter, DA. Rather, the electrochemical oxidation is rapid at the basal surface of highly orientated pyrolytic graphite (HOPG), but rapidly poisoned by the electro-oxidation process causing the adsorption of polymeric material at the electrode. We are able to take advantage of this in scanning electrochemical cell microscopy (SECCM),[7] by designing patterning experiments, such that the reaction is measured essentially on a pristine surface at high resolution, but as the SECCM probe moves on to a new location it leaves behind the blocking products as a place marker of the electrochemical measurements that can then be found and analyzed by complementary microscopy.[8] This enables the electrochemical response to be correlated unambiguously to the location on the carbon electrode surface, revealing structure-activity correlates with unprecedented (nanoscale) resolution.

We first investigated the electro-oxidation of DA on the macroscale. Using a Teflon cylinder that was gently placed on the HOPG surface to define a 3 mm diameter working electrode (WE), ten consecutive CVs were recorded at 5 second intervals for DA oxidation in 0.15 M phosphate buffered saline (PBS) solution (150 mM NaCl), pH 7.2, at 0.1 V s^{-1} with a Ag/AgCl (150 mM NaCl) reference electrode and platinum counter electrode. The highest quality HOPG was used, originating from Dr. A. Moore, Union Carbide (now GE Advanced Ceramics), which was kindly provided by Prof. R. L. McCreery (University of Alberta, Canada). The HOPG was carefully cleaved immediately before use with a razor blade, as described previously.[4] As we show herein, and as outlined in past work,[4,9] this procedure and material provides very high quality surfaces with very low step density and extensive basal terraces. Figure 1 shows typical CVs of (a) 1 mM and (b) 50 μM DA, with the first CV in each case recorded within 1 minute of freshly cleaving HOPG. For 1 mM DA, the initial CV shows an apparent quasi-reversible electrochemical response with a peak to peak separation of 68 mV, that rapidly deteriorates over the course of subsequent measurements. The basal surface is rapidly contaminated, as evident from the decrease in peak current by 80% and the dramatic increase in peak-to-peak separation to > 280 mV after 10 cycles. In contrast, by decreasing the concentration to 50 μM, the initial peak-to-peak separation is 30 mV, and the extent to which the signal decays is diminished over the following 10 cycles, although there is still some surface blocking, as detected by *in-situ* AFM, carried out whilst performing voltammetry. Figure 1c shows a typical image of the surface of HOPG in 50 μM DA (0.15 PBS, pH 7.2) after having performed just one CV between the potential limits of

0 V (start and end potential) and 0.45 V (reverse potential) at 0.1 V s^{-1}. The image shows coverage of the electrode surface by DA oxidation products, due to polymerization[1c] taking place.

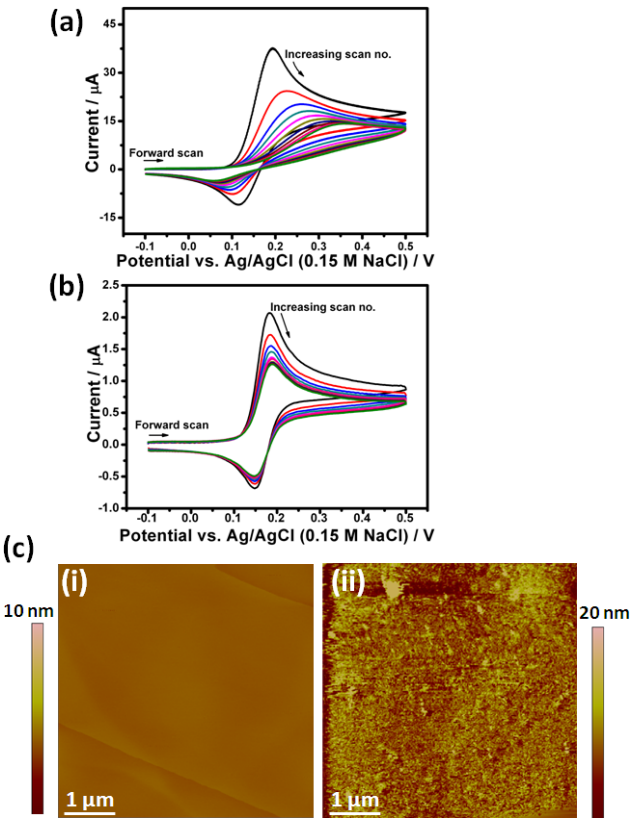

Figure 1. CVs for the oxidation of (a) 1 mM and (b) 50 µM DA at 0.1 V s^{-1} on pristine basal plane HOPG. (c) HOPG AFM images: (i) a pristine surface and (ii) *in-situ* image after one CV for 100 µM DA electro-oxidation between 0 and 0.45 V at 0.1 V s^{-1}.

Although these macroscopic data could suggest that the basal surface of HOPG is actually highly electrochemically active, in contrast to previous work,[4,5] the evidence is not definitive because the electrode comprises of a basal surface intersected by step edges. Thus, to determine definitively the surface sites for DA electro-oxidation, we used SECCM[7a,b,10] to image an area of the HOPG with a distinctive line-pattern, so that SECCM activity data could be compared with AFM and SEM measurements of the same area, to allow direct correlation of HOPG structure with the activity for DA electro-oxidation. For the studies reported first, a dual channel borosilicate pipet, pulled to a ~1 µm tapered end, was filled with 100 µM DA in 0.15 M PBS (150 mM NaCl), pH 7.2, so that a liquid meniscus formed at the end of the tip[7b] and Ag/AgCl quasi-reference counter electrodes (QRCEs) were inserted into each channel. The HOPG sample was mounted on a high-precision *xy*-piezoelectric stage and connected as the WE. When the tip was lowered using a *z*-piezoelectric positioner, so that the meniscus made contact with the WE, an electrochemical cell was formed[7a,b,8,10-11] (see Supporting Information, Figure S1). Using the SECCM setup, a linear sweep voltammogram (LSV) was run before patterning experiments; a typical example is shown in Figure 2a. The wave is sigmoidal, as expected of the SECCM format with a tapered pipet,[7b] reaching a limiting current of *ca.* 8 pA at ~0.3 V, a reasonable value based on the pipet dimensions, diffusion coefficient and concentration of DA.[7b] The separation between the ¼ and ¾ wave potentials is *ca*. 60 mV, indicating some small kinetic limitations, most likely due to some blocking of the electrode on this time scale with a static probe (*vide supra*).

SECCM line patterning was first carried out at a substrate potential of 0.25 V *vs.* Ag/AgCl (0.15 M NaCl) resulting in a current just below the maximum diffusion-limited value. A small oscillation of the tip position normal to the surface (20 nm peak amplitude, 233.6 Hz) was applied, giving rise to an alternating conductance current (AC) across the meniscus due to periodic changes in the meniscus height. This AC (~65 pA) was used as a set-point for feedback, enabling the tip to be kept at constant tip-to-substrate separation during imaging. The direct ion conductance current (DC) between the 2 QRCEs (Supporting Information, Figure S1) was ~3.2 nA. The resulting surface pattern is evident in Figures 2b-e: it covers 560 µm in length. With the tip scanned at a speed of 1 µm s^{-1}, with 78 data points recorded every second (each an average of 512 samples), > 40,000 individual measurements are made across the surface.

The SECCM surface activity map (Figure 2b) clearly show the HOPG surface currents are essentially constant at around 6.4 ± 1.0 pA over the probed area (see also Supporting Information, Figure S2 for a histogram of all activity data). The SECCM conductance currents (AC and DC), Figure 2c and d, are fairly constant and highlight that the probe maintains a fixed position from the surface and that mass transport is constant (see also Supporting Information, Figure S2, for histograms of all data). There are some small features that coincide in all 3 current maps (Figures 2b-d) along the *y* axis scan, which correspond to positions where the droplet encounters multilayer or monolayer steps causing small disruptions in the droplet size and surface interaction. However, these features are not significant. The simultaneously obtained topography map (tip position in *x*, *y*, and *z*) can also be found in Supporting Information (Figure S3), confirming the imaging of the surface.

As highlighted earlier, a key feature of the approach described is that the electro-oxidation of DA leads to the deposition of material, enabling current activity from SECCM to be linked unambiguously to the site on the WE. The AFM image in Figure 2e confirms that continuous deposition of the DA oxidative products occurred throughout the SECCM measurements. Note that the occasional streaking in the region of the deposited film (where the topography appears higher) is due to the AFM tip sticking and dragging the film. This is not true topography and is not seen in the scanning electron microscopy image of the same area (Supporting Information, Figure S4). Significantly, the AFM data show that the starting point of the deposition patterning (see Supporting Information, Figure S5, for a magnified view of this region) was initiated on a basal plane region, at least 2 µm away from the nearest step edge. This region, in the center of the spiral, evidently had associated high electrochemical activity indicating that the reactive patterning and corresponding HOPG electroactivity did not require a step defect but was solely due the electro-oxidation of DA on the basal plane.

More detailed AFM analysis on a section of the pattern (marked in Figure 2(e)) was carried out to allow correlation between activity and the HOPG surface structure. Figure 3(a) shows an AFM image of this region, along with the corresponding (b) surface activity (green) and DC component of the conductance current (blue). The AFM image

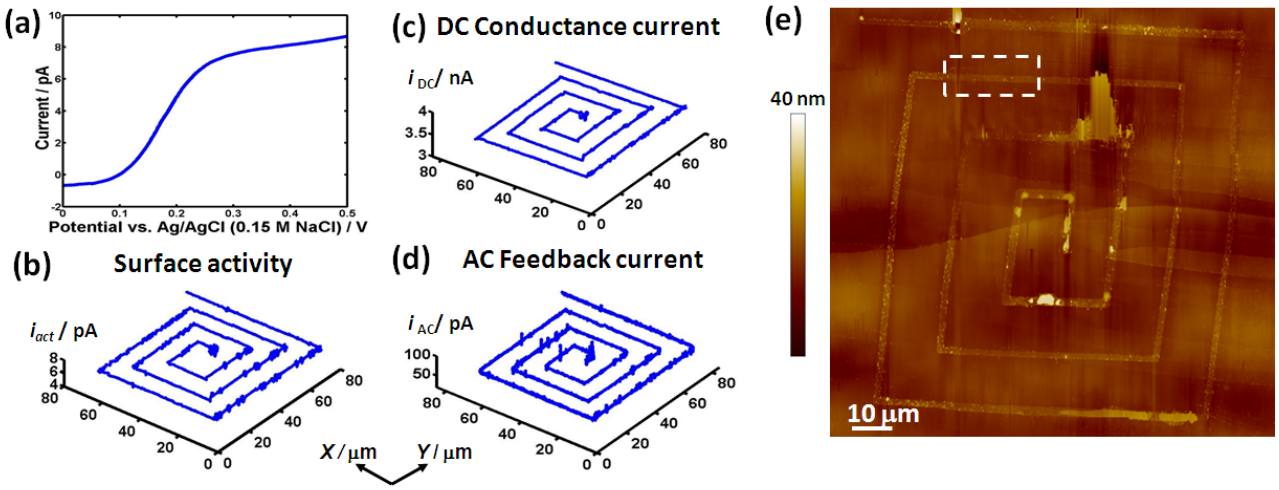

Figure 2. (a) SECCM linear sweep voltammogram for the oxidation of 100 µM DA (0.15M PBS) at 0.1 V s^{-1}. SECCM reactive patterning maps for DA electro-oxidation: (b) surface activity; (c) DC component of the conductance current; and (d) AC component of the conductance current used for feedback (see text for details). (e) AFM image of the HOPG surface showing the SECCM deposited pattern.

shows the deposited line essentially travels exclusively on a basal terrace with no obvious step defects. The corresponding SECCM data show uniform surface activity that remains fairly constant around 6.5 ± 0.1 pA as expected for a very active electrode surface.

Taken together, the data in Figure 3 show unequivocally that DA electro-oxidation occurs readily at the basal surface of HOPG, in complete contrast to the present model, which considers the basal surface to be inert, with step edges required to catalyze the reaction. For some other electrode materials, catechol adsorption has been shown to promote fast electron transfer,[12] and to elucidate whether this was important for the basal surface of HOPG, we carried out SECCM 'landing' transient chronoamperometric measurements in which the QRCEs in the pipet cell were biased at a value to promote DA oxidation when the meniscus came into contact with the pristine HOPG surface. Experiments were carried out with 10 µM DA to minimize any accumulation of DA on the surface. A typical transient, characteristic of 20 run on fresh spots on a pristine HOPG (AM) surface, is given in Supporting Information Figure S6. The redox current decayed to a steady-value on a timescale (few hundred milliseconds) characteristic of diffusion in SECCM.[13] While this indicates facile electron transfer we cannot rule out the involvement of DA adsorption, although the adsorption rate constant would need to be similar to or higher than measured on other carbon electrodes.[12b]

We were next interested in elucidating if there was any variation in activity between the basal surface and step edges and so SECCM reactive patterning was also carried out at a potential close to the half-wave potential, where any such variation would have been more readily evident. SECCM imaging was successful with 100 µM DA, but the diminished reaction flux meant that the electrodeposition was not sufficiently extensive for analysis by AFM. Note that the result of this experiment also confirms the patterning to be due to product adsorption and not the reactant. The concentration was thus increased to 300 µM. Figure 4a shows a typical line from DA electro-oxidation which travels along a large basal terrace as well as intersecting with several steps, ranging between 0.3 (monolayer) to 1.5 nm in height (see AFM cross-section overlaid (red) on Figure 4a). By correlating the AFM image with the DC component of the conductance current

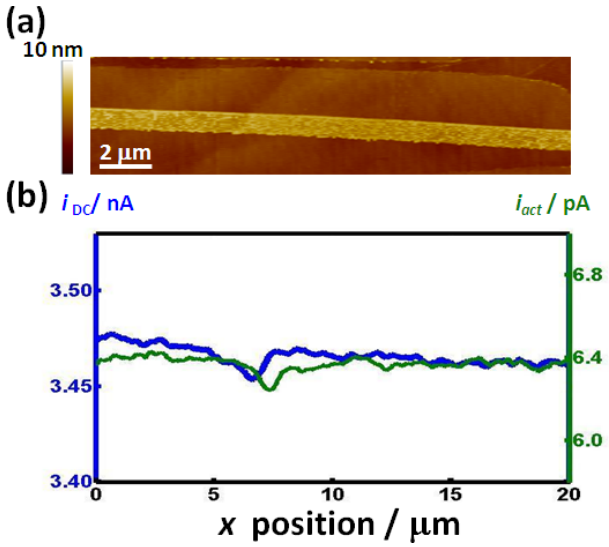

Figure 3. (a) 20 × 5 µm AFM image showing a section of the line patterning, marked in Figure 2(e), along with the corresponding surface activity (green) and DC component of the conductance current (blue) overlaid (b).

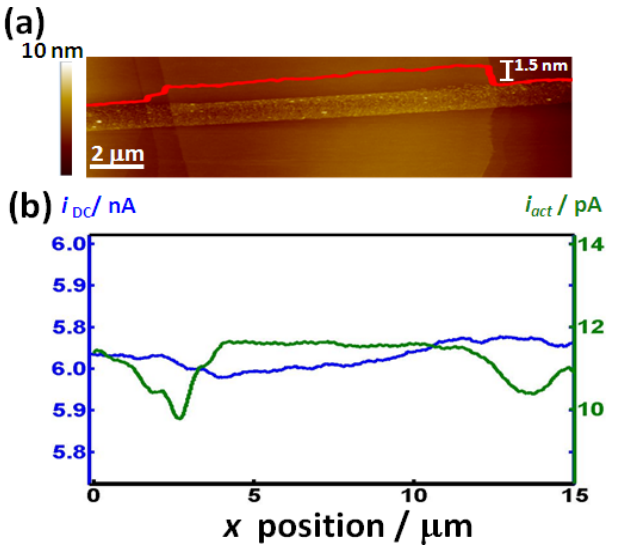

Figure 4. (a) 15 × 5 µm AFM image showing a section of line patterning carried out at the half-wave with 300 µM DA (0.15M PBS), with the AFM cross-section overlaid (red). The corresponding surface activity (green) and DC component of the conductance current (blue) shown in (b).

(blue) and the surface activity (green), as shown in Figure 4(b), the following important points can be made. First, it can be seen that as the meniscus travels along the basal terrace (approximately 9 μm long) the surface activity remains constant, at around 11 pA, a value consistent with a highly active surface. Second, in the region of step edges, the surface current drops slightly. Since the meniscus still mostly covers the basal surface in these regions, we attribute this to enhanced blocking of the surface in stepped regions on the SECCM timescale. It can be seen that the corresponding DC current (Figure 4b) is fairly uniform in this region, i.e. the mass transport rate is constant.

The major outcome of this study has been to show that the electro-oxidation of the model catechol, DA, occurs readily on basal plane HOPG, in contrast to the longstanding model that has pictured the basal plane as inert. However, the surface is easily contaminated by reaction products which leads to a rapid deactivation of the surface. SECCM reactive patterning is a new approach that allows precise correlation of surface activity with the character of the surface, providing unequivocal and unambiguous correlation of surface structure and electrochemical activity. Of course, the basal surface itself contains point defects that may have different local ET activity, but - as we have pointed out elsewhere[14] - such defects have never been considered necessary to explain the reactivity of HOPG. As the samples used for the studies herein were of the very highest quality in terms of low defect density,[14] our measurements represent the behavior of the best available pristine surface, which is essentially uniformly active on the SECCM scale. The approach provides a significant weight of evidence – in the form of thousands of individual current measurements that can be attributed unequivocally to the basal surface.

This new view of complex electrochemical processes at graphite, together with other recent studies on simpler redox systems,[10,13,14] suggests that a significant reappraisal of graphite as an electrode material is needed, with major implications for related sp^2 carbons, such as graphene and nanotubes. More generally, the study adds to a growing body of work highlighting the considerable value of electrochemical patterning and imaging[15] as a means of understanding local surface activity.

ASSOCIATED CONTENT

Supporting Information. Further SECCM data, AFM and SEM data. This material is available free of charge via the Internet at http://pubs.acs.org.

AUTHOR INFORMATION

Corresponding Author

* To whom correspondence should be addressed. E-mail: p.r.unwin@warwick.ac.uk.

ACKNOWLEDGMENT

We are grateful to the European Research Council (ERC-2009-AdG 247143-QUANTIF) and EPSRC for a studentship to ANP (Analytical Fund EP/F064861/1e). EPSRC supported KM by funding of the MOAC Doctoral Training Centre. Some equipment used in this research was obtained through Birmingham Science City with support from Advantage West Midlands and the European Regional Development Fund. We thank Prof. R. L. McCreery for kindly providing the high quality HOPG sample used for the studies herein. We are grateful to Dr. A. W. Colburn for designing and building electronic instrumentation.

REFERENCES

(1) (a) McCreery, R. L. *Chem. Rev.* **2008**, *108*, 2646; (b) Jacobs, C. B.; Peairs, M. J.; Venton, B. J. *Anal. Chim. Acta* **2010**, *662*, 105; (c) Yang, X.; Haubold, L.; DeVivo, G.; Swain, G. M. *Anal. Chem.* **2012**, *84*, 6240; (d) Hawley, M. D.; Tatawawadi, S. V.; Piekarski, S.; Adams, R. N. *J. Am. Chem. Soc.* **1967**, *89*, 447-50.
(2) (a) Yu, X.; Wang, Q.; Lin, Y.; Zhao, J.; Zhao, C.; Zheng, J. *Langmuir* **2012**, *28*, 6595; (b) Güell, A. G.; Meadows, K. E.; Unwin, P. R.; Macpherson, J. V. *Phys. Chem. Chem. Phys.* **2010**, *12*, 10108; (c) Singh, Y. S.; Sawarynski, L. E.; Michael, H. M.; Ferrell, R. E.; Murphey-Corb, M. A.; Swain, G. M.; Patel, B. A.; Andrews, A. M. *ACS Chem. Neurosci.* **2010**, *1*, 49.
(3) (a) Zhou, M.; Zhai, Y.; Dong, S. *Anal. Chem.* **2009**, *81*, 5603;(b) Wightman, R. M. *Science* **2006**, *311*, 1570;(c) Day, J. J.; Roitman, M. F.; Wightman, R. M.; Carelli, R. M. *Nat. Neurosci.* **2007**, *10*, 1020;(d) Alwarappan, S.; Erdem, A.; Liu, C.; Li, C.-Z. *J. Phys. Chem. C* **2009**, *113*, 8853.
(4) Kneten, K. R.; McCreery, R. L. *Anal. Chem.* **1992**, *64*, 2518.
(5) (a) Bowling, R. J.; Packard, R. T.; Mccreery, R. L. *J. Am. Chem. Soc.* **1989**, *111*, 1217;(b) Kachoosangi, R. T.; Compton, R. G. *Anal. Bioanal. Chem.* **2007**, *387*, 2793.
(6) (a) Sudhakara Prasad, K.; Muthuraman, G.; Zen, J.-M. *Electrochem. Commun.* **2008**, *10*, 559;(b) Lim, C. X.; Hoh, H. Y.; Ang, P. K.; Loh, K. P. *Anal. Chem.* **2010**, *82*, 7387;(c) Strand, A. M.; Venton, B. J. *Anal. Chem.* **2008**, *80*, 3708.
(7) (a) Lai, S. C. S.; Dudin, P. V.; Macpherson, J. V.; Unwin, P. R. *J. Am. Chem. Soc.* **2011**, *133*, 10744;(b) Snowden, M. E.; Güell, A. G.; Lai, S. C. S.; McKelvey, K.; Ebejer, N.; O'Connell, M. A.; Colburn, A. W.; Unwin, P. R. *Anal. Chem.* **2012**, *84*, 2483;(c) Ebejer, N.; Schnippering, M.; Colburn, A. W.; Edwards, M. A.; Unwin, P. R. *Anal. Chem.* **2010**, *82*, 9141.
(8) Patten, H. V.; Lai, S. C.; Macpherson, J. V.; Unwin, P. R. *Anal. Chem.* **2012**, *84*, 5427.
(9) Chang, H.; Bard, A. J. *Langmuir* **1991**, *7*, 1143.
(10) Lai, S. C. S.; Patel, A. N.; McKelvey, K.; Unwin, P. R. *Angew. Chem. Int. Ed.* **2012**, *51*, 5405.
(11) (a) Güell, A. G.; Ebejer, N.; Snowden, M. E.; Macpherson, J. V.; Unwin, P. R. *J. Am. Chem. Soc.* **2012**, *134*, 7258;(b) Güell, A. G.; Ebejer, N.; Snowden, M. E.; McKelvey, K.; Macpherson, J. V.; Unwin, P. R. *Proc. Natl. Acad. Sci. USA* **2012**. *109*, 11487.
(12) (a) DuVall, S. H.; McCreery, R. L. *J. Am. Chem. Soc.* **2000**, *122*, 6759-6764. (b) (1) Bath, B. D.; Michael, D. J.; Trafton, B. J.; Joseph, J. D.; Runnels, P. L.; Wightman, R. M. *Anal. Chem.* **2000**, *72*, 5994-6002.
(13) (a) Anne, A.; Cambril, E.; Chovin, A.; Demaille, C.; Goyer, C. *ACS Nano* **2009**, *3*, 2927;(b) Edwards, M. A.; Bertoncello, P.; Unwin, P. R. *J. Phys. Chem. C* **2009**, *113*, 9218;(c) Williams, C. G.; Edwards, M. A.; Colley, A. L.; Macpherson, J. V.; Unwin, P. R. *Anal. Chem.* **2009**, *81*, 2486;(d) Frederix, P. L.; Bosshart, P. D.; Akiyama, T.; Chami, M.; Gullo, M. R.; Blackstock, J. J.; Dooleweerdt, K.; de Rooij, N. F.; Staufer, U.; Engel, A. *Nanotechnology* **2008**, *19*, 384004.
(14) Patel, A. N.; Collignon, M. G.; O'Connell, M. A.; Hung, W. O. Y.; McKelvey, K.; Macpherson, J. V.; Unwin, P. R. *J. Am. Chem. Soc.*[Just accepted] D.O.I. 10.1021/ja308615h
(15) (a) Hazimeh, H.; Nunige, S.; Cornut, R.; Lefrou, C.; Combellas, C.; Kanoufi, F. *Anal Chem* **2011**, *83*, 6106-13. (b) Nunige, S.; Cornut, R.; Hazimeh, H.; Hauquier, F.; Lefrou, C.; Combellas, C.; Kanoufi, F. *Angew Chem Int Ed Engl* **2012**, *51*, 5208. (c) Shan, X.; Patel, U.; Wang, S.; Iglesias, R.; Tao, N. *Science* **2010**, *327*, 1363.

TOC